SOFT ROBOTS

Fast and programmable locomotion of hydrogel-metal hybrids under light and magnetic fields

Chuang Li[1]*, Garrett C. Lau[1,2]*, Hang Yuan[1,3]*, Aaveg Aggarwal[1,2], Victor Lopez Dominguez[4], Shuangping Liu[1,2], Hiroaki Sai[1], Liam C. Palmer[1,5,10], Nicholas A. Sather[2], Tyler J. Pearson[1,5], Danna E. Freedman[1,5], Pedram Khalili Amiri[4], Monica Olvera de la Cruz[1,2,5,6,7†], Samuel I. Stupp[1,2,5,8,9,10†]

The design of soft matter in which internal fuels or an external energy input can generate locomotion and shape transformations observed in living organisms is a key challenge. Such materials could assist in productive functions that may range from robotics to smart management of chemical reactions and communication with cells. In this context, hydrated matter that can function in aqueous media would be of great interest. Here, we report the design of hydrogels containing a scaffold of high–aspect ratio ferromagnetic nanowires with nematic order dispersed in a polymer network that change shape in response to light and experience torques in rotating magnetic fields. The synergistic response enables fast walking motion of macroscopic objects in water on either flat or inclined surfaces and also guides delivery of cargo through rolling motion and light-driven shape changes. The theoretical description of the response to the external energy input allowed us to program specific trajectories of hydrogel objects that were verified experimentally.

INTRODUCTION

The design of hydrated soft matter that responds to external stimuli with motion and shape changes inspired by living organisms remains an important scientific challenge. Design of hydrated structures and mechanisms to achieve this objective may be eventually useful for the development of materials with locomotive capacity for aqueous chemistry or to augment the functions of living systems (*1*–*3*). Pursuing this objective with magnetically actuated soft matter is particularly attractive because magnetic fields can safely penetrate most materials, including biological matter. In previous work, it has been shown that magnetic fields can remotely bend metallic backbones and induce walking (*4*), activate locomotion of particle filaments (*5*, *6*), and induce motion of elastomeric materials that contain ferromagnetic components (*7*–*11*). In these elastomeric materials, specific patterns of magnetization and object geometry were generated by various fabrication techniques. However, once these samples have been prepared, the responsive magnetization profile is static and cannot be reconfigured in the absence of a magnetic field. The magnetic components widely used in previous work were spherical and irregularly shaped magnetic particles (such as iron oxide and NdFeB) that lack magnetic anisotropy (*7*, *8*, *10*, *11*) and thus require a high loading of magnetic material or the use of strong fields to activate a considerable response. The matrices used to embed these particles have been hydrophobic polymers (*12*), elastomers (*7*, *8*), or particles supported on rigid silicon nitride membranes (*9*). Hydrogels offer the possibility to function in water and also have the capacity to exchange fluids with aqueous environments (*13*). Previous work on macroscopic hydrogels has shown bending, walking, or swimming behavior activated by light (*14*–*16*), thermal (*17*), chemical (*18*), or electrochemical stimuli (*19*), but all of these systems displayed slow actuation kinetics for locomotion unless they were scaled down to the micrometer scale (*20*). Incorporation of functional nanoscale components into hydrogels provides a powerful strategy to generate emergent properties and performance (*21*–*23*). By incorporating high–aspect ratio nickel (Ni) nanowires into a photoactive hydrogel, we report here on the development of anisotropic hydrogel-metal hybrid materials that are actuated by magnetic fields after exposure to light that also remain reconfigurable by light to alter their magnetic response. We theoretically predict the response of the hybrid objects to light and magnetic fields enabling the programming of their trajectories under water and gait on the fly.

In addition to magnetically driven actuation described above, light as a stimulus is also useful because it can be delivered to synthetic matter remotely and potentially in localized fashion (*24*). Previous investigators have incorporated different photoactive components such as photothermal agents (*12*) and molecular photoswitches (*25*) into hydrogels to fine-tune their chemical and physical properties. Molecular photoswitches are unique because they can be wavelength-selective and reversibly reconfigure conformations upon irradiation. Recent examples of light-responsive materials include polymer films containing cis-trans azobenzene switches (*26*) and hydrogels based on spiropyran (SP) chemistry (*15*, *16*, *27*, *28*) or molecular motors (*29*, *30*). Soft materials capable of responding to both light and magnetic fields can initiate the exploration in soft matter of the multisensory interactions we observe in living organisms (*12*). In this work, we designed and synthesized hydrogel objects that perform distinct tasks with remote control over geometry, stiffness, and magnetization using a combination of light and magnetic fields. The samples are prepared by incorporating aligned high–aspect ratio ferromagnetic nanowires into a photoactive hydrogel matrix that is

[1]Center for Bio-inspired Energy Science, Northwestern University, 2145 Sheridan Road, Evanston, IL 60208, USA. [2]Department of Materials Science and Engineering, Northwestern University, 2220 Campus Drive, Evanston, IL 60208, USA. [3]Graduate Program in Applied Physics, Northwestern University, 2145 Sheridan Road, Evanston, IL 60208, USA. [4]Department of Electrical and Computer Engineering, Northwestern University, 2145 Sheridan Road, Evanston, IL 60208, USA. [5]Department of Chemistry, Northwestern University, 2145 Sheridan Road, Evanston, IL 60208, USA. [6]Department of Chemical and Biological Engineering, Northwestern University, 2145 Sheridan Road, Evanston, IL 60208, USA. [7]Department of Physics and Astronomy, Northwestern University, 2145 Sheridan Road, Evanston, IL 60208, USA. [8]Department of Biomedical Engineering, Northwestern University, 2145 Sheridan Road, Evanston, IL 60208, USA. [9]Department of Medicine, Northwestern University, 676 N St. Clair Street, Chicago, IL 60611, USA. [10]Simpson Querrey Institute, Northwestern University, Chicago, IL 60611, USA.
*These authors contributed equally to this work.
†Corresponding author. Email: m-olvera@northwestern.edu (M.O.d.l.C.); s-stupp@northwestern.edu (S.I.S.)

capable of changing shape in response to light. Macroscopic bending of the hydrogel upon light irradiation deforms existing magnetization profiles, which results in complex three-dimensional (3D) magnetization that leads to programmable actuation. These hydrogels can perform functions such as walking, steering, climbing, and delivering cargo under the control of an external magnetic field and light (Movie 1). Furthermore, small changes in the chemical structure of these systems change the kinetics of light response and thus provide access to a broader range of actuating behaviors.

RESULTS

Design of the hydrogel-metal hybrid

To synthesize the hydrogel-metal samples, Ni nanowires (fig. S1) were added to a solution containing monomers, cross-linking agents, initiators, and a polymerizable photoswitching SP monomer (SP1; scheme S1) to create a light-responsive cross-linked network (Fig. 1A and fig. S2; see Materials and Methods for synthetic details). Under dark and acidic conditions, the photoswitch contains a hydrophilic protonated merocyanine (MCH^+) moiety that isomerizes to a hydrophobic SP form upon exposure to visible light. This isomerization with light exposure results in contraction of the hydrogel because of dehydration, followed by expansion under dark conditions. The ferromagnetic nanowires were aligned under a static magnetic field and then fixed in this configuration by free-radical photopolymerization of the light-responsive hydrogel (Fig. 1, A and B, and figs. S3 and S4). Small-angle x-ray scattering (SAXS) confirmed the alignment of the nanowires, as shown by the radial integration of a 2D scattering intensity plot (Fig. 1C). We measured a remnant magnetization of 260 electromagnetic units/cm^3 parallel to the alignment of the nanowires, and the coercive magnetic field required to reverse the magnetization of the sample was found to be 25 mT (Fig. 1D). This is a 1.9-fold enhancement in the coercivity over bulk nickel (13 mT) (*31*), highlighting the utility of the shape anisotropy derived from the nanowire architecture (~8 μm long on average and 200 nm in diameter). In comparison, magnetization loops measured perpendicular to the alignment direction were noisy and exhibited a much lower magnetization, demonstrating the magnetic anisotropy of the composite material. Samples containing randomly oriented Ni nanowires did not show any macroscopic magnetic anisotropy (fig. S5). Also, when spherical Ni nanoparticles formed chained clusters during photopolymerization under a magnetic field, we did not detect any anisotropy because each individual particle can rotate to align its magnetization with the field (fig. S6). The magnetic anisotropy of the Ni nanowires was also confirmed by superconducting quantum interference device magnetometry with a rotating stage (fig. S7). This indicates that the shape of Ni nanowires is a critical structural feature responsible for the anisotropic magnetic properties of the Ni-hydrogel composites.

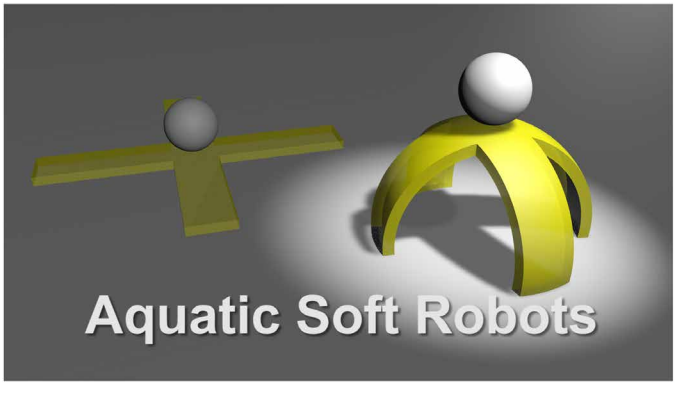

Movie 1. Overview of programmable aquatic hydrogel robots.

Dual response to light and magnetic fields

The as-prepared hydrogel materials were soaked in acidic water for 40 min to obtain an equilibrated swollen state before photo-actuation experiments in a large water bath (~100 ml) that contained 5 mM HCl. Upon light exposure, this swollen state underwent a shrinkage to 84% of its original volume (fig. S8). Because the actuation occurs in acidic water, the SP1 hydrogel is capable of sequential actuation cycles that did not require additional HCl preconditioning. We found that the flat hydrogel object bends toward the light source upon irradiation from one side and recovers its original flat geometry in the dark. This bending-flattening process is highly reversible, and the hydrogel could maintain its photoactivity with the same maximum bending angle over at least 10 cycles by switching the light on and off (see fig. S9). The fundamental mechanism of deformation under the action of light in the materials investigated is rooted in the creation of a spatial gradient in the population of hydrophilic and hydrophobic moieties within the hydrogel (MCH^+ versus SP segments). This should result in a decrease of water concentration within the material as the density of SP units increases, leading, in turn, to mechanical deformation, either bending up or down depending on the irradiation direction. A phenomenological model (*32*) has been developed to describe such photoinduced hydrophobicity in gels with an additional contribution to the free energy proportional to $r_{sp}(1-\phi)$, where ϕ is the monomer volume fraction and r_{sp} is the fraction of chromophores in the SP configuration. Here, we derived the additional contribution to be $\alpha\phi(1-\phi)$, where α is given by

$$\alpha = \frac{zf}{k_B T}(u_{sw} - u_{mw})\, r_{sp}$$

where u_{sw} and u_{mw} are the interaction energies of the SP and MCH^+ moieties with water, respectively; z is the coordination number of the lattice; and f is the fraction of monomers containing a chromophore. Moreover, r_{sp} is described by the kinetics of the chemical reaction, $MCH^+ \leftrightarrow SP$, and can be calculated by computing the light intensity as a function of spatial coordinates in the hydrogel objects (see the Supplementary Materials for details). Figure 1E (left) shows the calculated water concentration gradient within a hydrogel slab using this methodology and the resultant deformation. The deformed light-induced bent geometry leads to a nonuniform 3D magnetization profile of the magnetic nanowires (indicated by the magenta arrows) with respect to the applied magnetic field. This change enables the arch-shaped hydrogel to respond to a spatially uniform external magnetic field $\mathbf{B_{ext}}$ but remains completely unresponsive in its flat state. Thus, the span of the arch-shaped hydrogel can be increased or decreased by simply applying a static magnetic field parallel or anti-parallel to the nanowires' alignment direction (Fig. 1E, right). To quantitatively characterize deformations of the hydrogel, we developed a continuum model of fiber-reinforced magnetoelastic materials. An external magnetic field induces local torques because Ni nanowires prefer to align with the field. We solve Maxwell's equations in the limit of a static magnetic field (the magnetostatics) to obtain the distribution of the magnetic flux density $\boldsymbol{B}$, which couples with the magnetization of Ni nanowires and creates magnetic torques on the

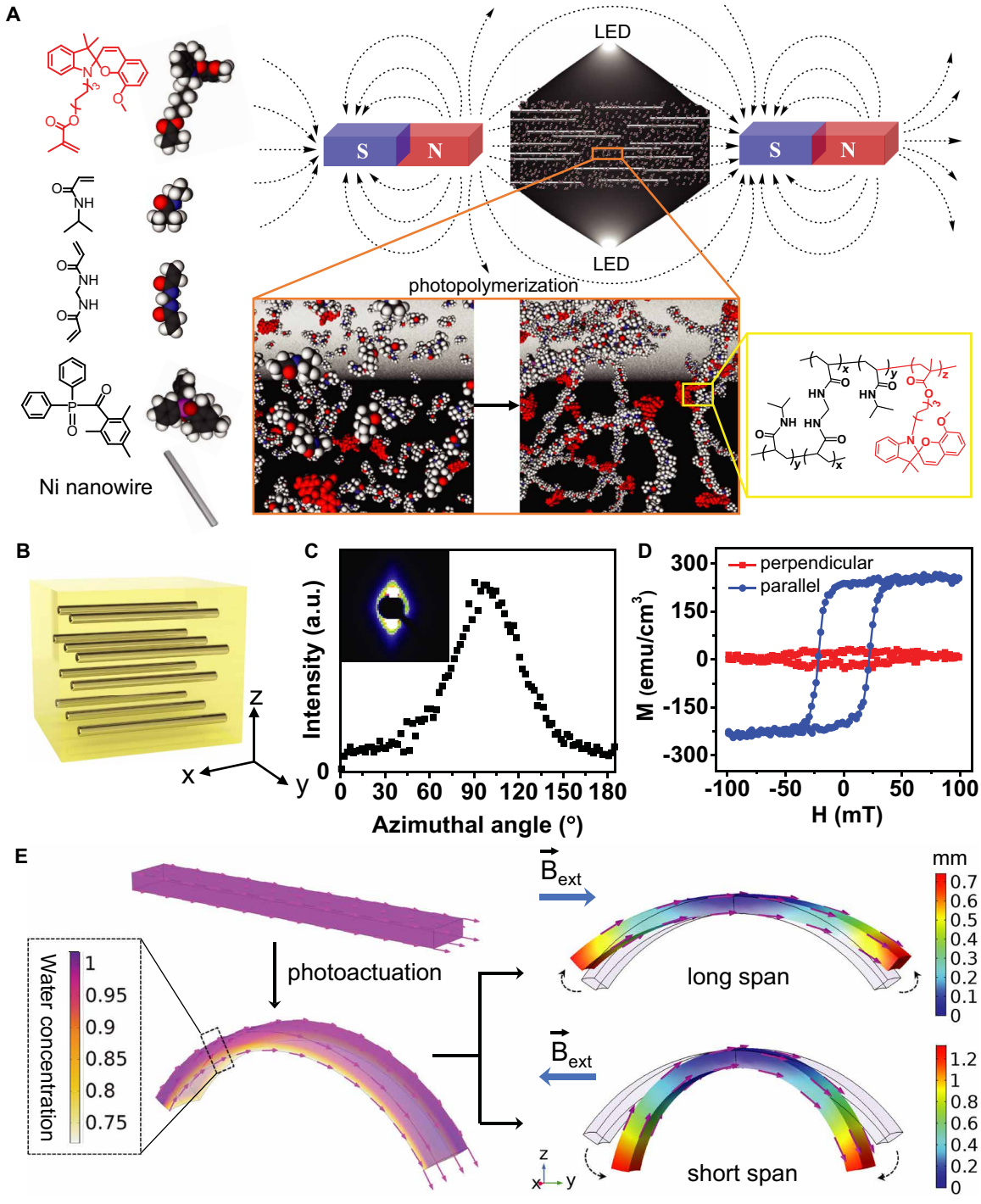

Fig. 1. Hydrogels designed for coupled response to light and magnetic fields. (**A**) Schematic of Ni nanowires aligned and fixed within a hydrogel network containing photoactive SP moieties using a uniform magnetic field during free radical photopolymerization. (**B**) Schematic representation of aligned Ni nanowires (gray) immobilized in a hydrogel network (yellow). (**C**) Radial integration of 2D SAXS pattern (inset) revealing the macroscopic alignment of Ni nanowires within the hydrogel. (**D**) Magnetization loops parallel and perpendicular to the alignment axis of the nanowires. (**E**) Finite element calculation of the water concentration gradient and deformation in a slab of hydrogel exposed to light (left); finite element calculation of deformation as a result of magnetic field exposure in a hydrogel slab previously bent by light (right). Magenta arrows denote the magnetization of Ni nanowires; blue arrows indicate the direction of the external magnetic fields; dashed arrows represent the movement of both ends after applying magnetic fields; rainbow surface colors represent the deformations relative to its initial configurations (shaded regions).

nanowires (see the Supplementary Materials). Given that the nanowires are immobilized by the hydrogel (fig. S3), these magnetic torques transmit stresses that collectively result in macroscopic deformation of the material. Because the interaction between the field and magnetized material is orientation dependent, strain tensors are not enough to fully describe the state of the system. Instead, we used here the deformation gradient tensor $\boldsymbol{F}$, which takes into account the rotational deformation to develop a free energy density function of fiber-reinforced magnetoelastic materials, W, given by

$$W = \frac{1}{2}\mu(\overline{I_1} - 3) + \frac{1}{2}\mu\gamma(\overline{I_4} - 1)^2 + \frac{\kappa}{2}(J-1)^2 - (\boldsymbol{FM})\cdot\boldsymbol{B}$$

where μ and κ are the shear and bulk modulus, respectively; γ is a stiffness parameter resulting from mechanical reinforcement by the aligned nanowires (*33*); J = det $\boldsymbol{F}$ characterizes volumetric changes with respect to the initial state; $\overline{I_1}$ describes shape changes and $\overline{I_4}$ describes the deformation along the direction of nanowires; $\boldsymbol{B}$ is the magnetic flux density; and $\boldsymbol{M}$ is the magnetization field in the reference configuration (see the Supplementary Materials for details). The magnetic energy term $W_m = -(\boldsymbol{FM})\cdot\boldsymbol{B}$ corresponds to the magnetic stress tensor $\boldsymbol{\sigma}_m = \frac{1}{J}\frac{\partial W_m}{\partial \boldsymbol{F}}\boldsymbol{F}^T = -J^{-1}\boldsymbol{B}\otimes\boldsymbol{FM}$. This model demonstrates a clear coupling between light and magnetic actuation via elastic deformation. With light exposure, the light propagates through the hydrogel and creates differential shrinking, which induces macroscopic deformations ($\boldsymbol{F}$) of the hydrogel and enables the light actuation. Because the Ni nanowires are trapped within the hydrogel, the elastic deformation will change the spatial orientation of Ni nanowires ($\boldsymbol{FM}$). This change in Ni nanowire orientation ultimately modifies magnetic actuation ($\boldsymbol{\sigma}_m$). In this model, the nickel nanowires move with the hydrogel without slipping, and the higher-order energy contributions in $\boldsymbol{B}$ to the free energy density W are ignored (*8*). The strength of external magnetic field stays in the linear response region of Ni nanowires (fig. S10), and all elastic parameters are calibrated from experimental measurements (fig. S11). This continuum model

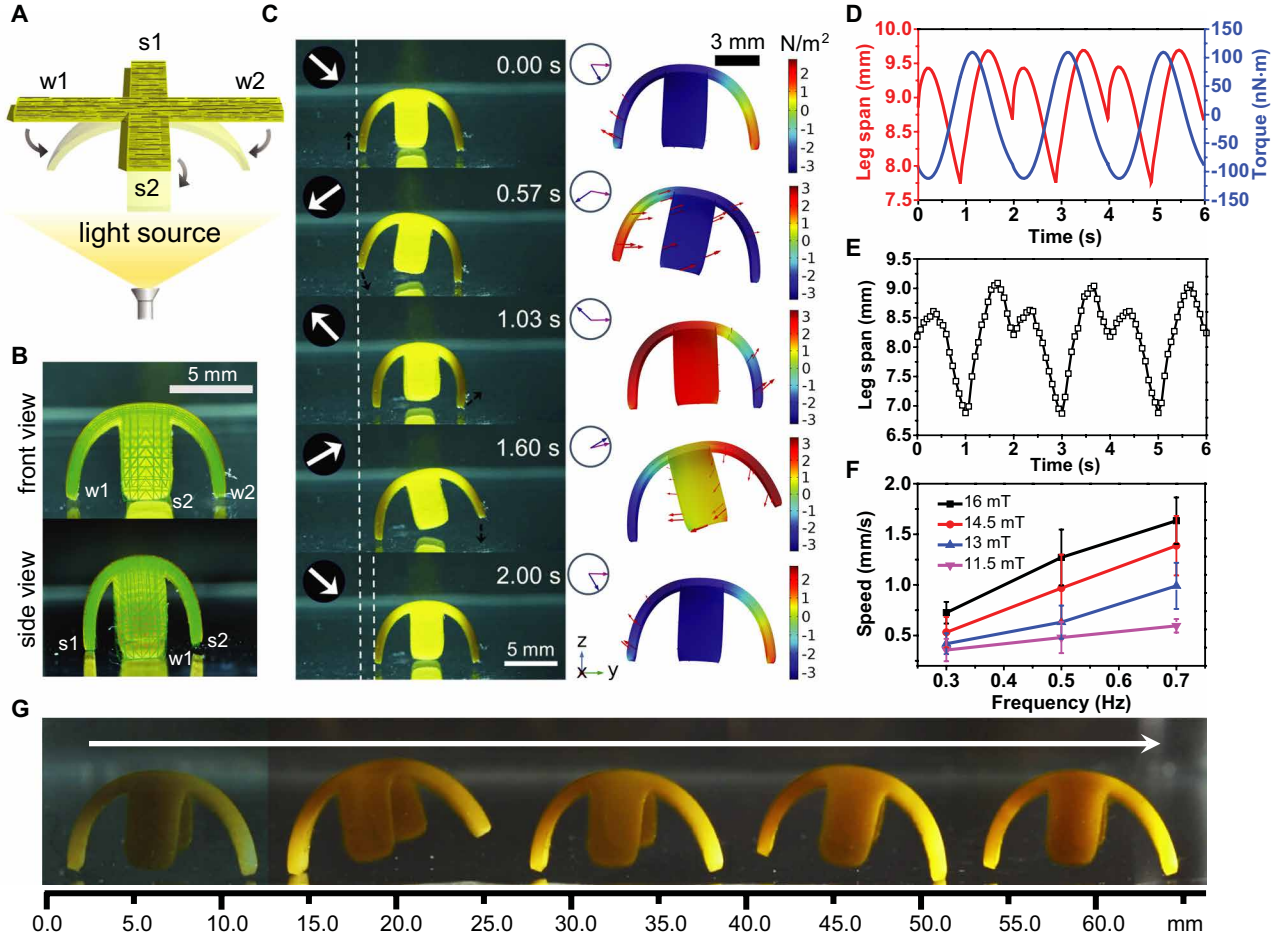

Fig. 2. Light triggered walking under rotating magnetic fields. (**A**) Schematic of a cross-shaped hydrogel film containing aligned Ni nanowires irradiated from below. (**B**) Photographs of the bent hydrogels (front and side views) superimposed with green wireframe representations of the calculated photo-actuation using a finite element method. (**C**) Left, photographs of the hydrogel walking from left to right for one cycle (white arrows indicate direction of the magnetic fields); right, calculated snapshots from a finite element simulation of the walking motion (color scale represents the *x* component of the magnetic torque density). Red arrows indicate instantaneous velocity field, blue arrows indicate direction of the external magnetic field, and magenta arrows indicate direction of the average magnetization. (**D**) Plot of the *x* component of the magnetic torque (blue) and leg span (red) from the simulation. (**E**) Plot of the experimental leg span of samples as a function of time over multiple walking cycles. (**F**) Plot of the walking speed as a function of rotating frequency at various magnetic field strengths (error bars represent SDs from three separate samples). (**G**) Time-lapse photographs of hydrogel walking (collected every four cycles, ~8.3 s) over macroscopic distances under a rotating magnetic field (14.5 mT, 0.7 Hz).

was solved using finite element methods and benchmarked with analytic solutions (fig. S12). It provides a quantitative analysis for the dynamic behavior of the hydrogels in magnetic fields.

Programmed walking and steering motions

To develop robotic functions, we prepared cross-shaped hydrogel films containing aligned Ni nanowires (Fig. 2A). The film thickness was fixed around 0.5 mm to obtain an optimal photoisomerization speed and deformation stability based on our previous results (*28*). After light irradiation, the flat sample bends up as an object with two walking legs (w1, w2) and two stabilizing arms (s1, s2) (Fig. 2B). The alignment of the wires within the object creates an anisotropic mechanical response, and therefore, the span between w1 and w2 (see front view) is larger than that between s1 and s2 (see side view). We calculated photo-actuation of these samples using the model described before and generated the green wireframes shown in Fig. 2B. The wireframes overlap exactly with the actual bending geometry of the hydrogels, observed from both front and side views, suggesting clear agreement between the calculated and actual light-induced deformation observed in the photographs. It is therefore possible to exploit this mechanical anisotropy (figs. S13 and S14) caused by the aligned Ni nanowires to modulate photo-actuation in hydrogel samples with simple geometries such as squares (fig. S15). We found that when the hydrogel-metal hybrids are illuminated and bent by the light, a nonuniform 3D magnetization profile is established that enables walking under the influence of an external rotating magnetic field (Fig. 2C and movie S1). As a control, samples containing unaligned Ni nanowires or aligned chains of Ni nanoparticles exhibited minimal movement under the same magnetic field and were not capable of walking (fig. S16). The average magnetization (purple arrow) and the external magnetic field (blue arrow) lie within the *y*-*z* plane, and the magnetic torque density is given by $\boldsymbol{\tau}_m = \boldsymbol{FM}/J \times \boldsymbol{B}$. Therefore, only the *x* component of the magnetic torque is a nonzero quantity. The rotating magnetic field in the *y*-*z* plane generates an oscillatory *x* component of the magnetic torque that causes the objects to rotate alternately clockwise and counterclockwise around the *x* axis (perpendicular to the walking direction) (Fig. 2D). Because of the combination of magnetic torque and gravity, the object lands on its front and back legs in alternating fashion (Fig. 2C). Our model assumes that the friction between the legs and the floor is large enough to avoid slippage during walking (see the Supplementary Materials for details). Magnetoelastic coupling results in a periodic change in the hydrogel's leg span (distance between w1 and w2) (Fig. 2, D and E), which enables the net displacement of the hydrogel along the *y* axis. Furthermore, longer side arms were found to be important in stabilizing the hydrogel's movement and optimizing its lift during walking because of a larger magnetic torque (movie S2 and fig. S17). Also, the walking speed was found to be faster with higher frequencies (0.3 to 0.7 Hz) or stronger magnetic fields (11.5 to 16.0 mT) (Fig. 2F and movie S3). With a fixed frequency (0.7 Hz) and field strength (14.5 mT), it was possible to achieve walking over macroscopic distances (~53 mm) (Fig. 2G) and reduction of the hydrogels to millimeter-size scales did not change the mechanism of motion (movie S4).

The hybrid hydrogels can also achieve steering motion in arbitrary directions while walking along the *x*-*y* plane by controlling the applied magnetic field to produce an additional torque in the *z* direction (i.e., normal to the walking plane). Using simulations, we predicted that the objects could turn 90° in 30° increments (Fig. 3A and movie S5) by programming the applied field in the *x*, *y*, and *z* directions to achieve the required torque (Fig. 3, B and C). The predicted motion using simulations was observed experimentally as shown in Fig. 3A. The two modes of motion (walking and steering) allow our hydrogel sample to reach any arbitrary destination on a 2D level or inclined surface. Figure 3D shows a designed arbitrary path with multiple turns, and Fig. 3E shows its corresponding experimental realization (movie S6). We therefore conclude that the experimental samples of these materials can have robotic functions, which in this case involve following continuous paths over macroscopic distances.

Effect of photoswitch chemistry on walking trajectories

To develop more complex robotic functions, we synthesized hydrogels with different molecular photoswitches (see the Supplementary Materials for synthetic details) to tune the kinetics of photo-actuation. Hydrogels made of SP1 can maintain their bending curvature under variable light intensities (96 to 190 mW/cm^2) through the duration of our experiments (Fig. 4A), confirmed by the change of leg span (Fig. 4C, black). We also synthesized a photoswitch (SP2) that could be covalently incorporated in the polymeric network, which lacks the methoxy group and displays faster photoisomerization to the closed ring form (figs. S18 and S19). The hydrogel component of the hybrid samples containing SP2 bend and then flatten in response to relatively low light intensities (23.5 to 33.0 mW/cm^2) (Fig. 4, B and C, red), because prolonged irradiation destroys the initial light-induced hydrophobicity gradient associated with bending of the material. Because the bending angle is highly tunable by changing irradiation conditions (fig. S20) and the walking behaviors depend directly on the bending geometry, a permanent walker made of SP1 walks with a constant speed, whereas one made of SP2 gradually loses its walking ability with continuous irradiation (Fig. 4D, fig. S21, and movie S7) and is therefore a transient walker. Note that the walking speed of SP2 samples has a large SD, probably because of the rapidly increasing stiffness upon light irradiation (fig. S14) as well as some uncontrolled slippage and rotation of the walker. The walking speed can be controlled by programmed sequences of light intensity. As shown in Fig. 4 (E and F), samples containing SP1 hydrogel were found to bend and walk faster as the light intensity increased. The walking speed of SP1 hydrogels after 10 min of sequential irradiation at low and then higher intensity (see Fig. 4F) was faster (1.2 mm/s) than the speed after 10 min of exposure to a constant light intensity (0.7 mm/s) (Fig. 4D). We suggest that light irradiation history leads to variations in bending curvature and mechanical properties. For example, Fig. 4 (E and F) shows plateaus in leg span and walking speed during the first 10 min. A full understanding of this phenomenon is beyond the scope of this paper, but we can suggest that equilibration rate of structures during irradiation will be sensitively dependent to light exposure history. Also, the SP1 hydrogel was able to selectively bend and its walking accelerated along a section of its path where the light source was localized (movie S7), offering another possibility for adaptive response to the surrounding environment. This permanent walker gradually stops walking when light is turned off (fig. S22), because the bending hydrogel returns to its initial flat geometry and the hydrophobicity gradient disappears. In contrast to the SP1 samples, prolonged light irradiation of SP2 leads to rapid penetration of light and the disappearance of the hydrophobicity gradient through the thickness of samples. Therefore, increasing the light intensity did not cause samples containing SP2

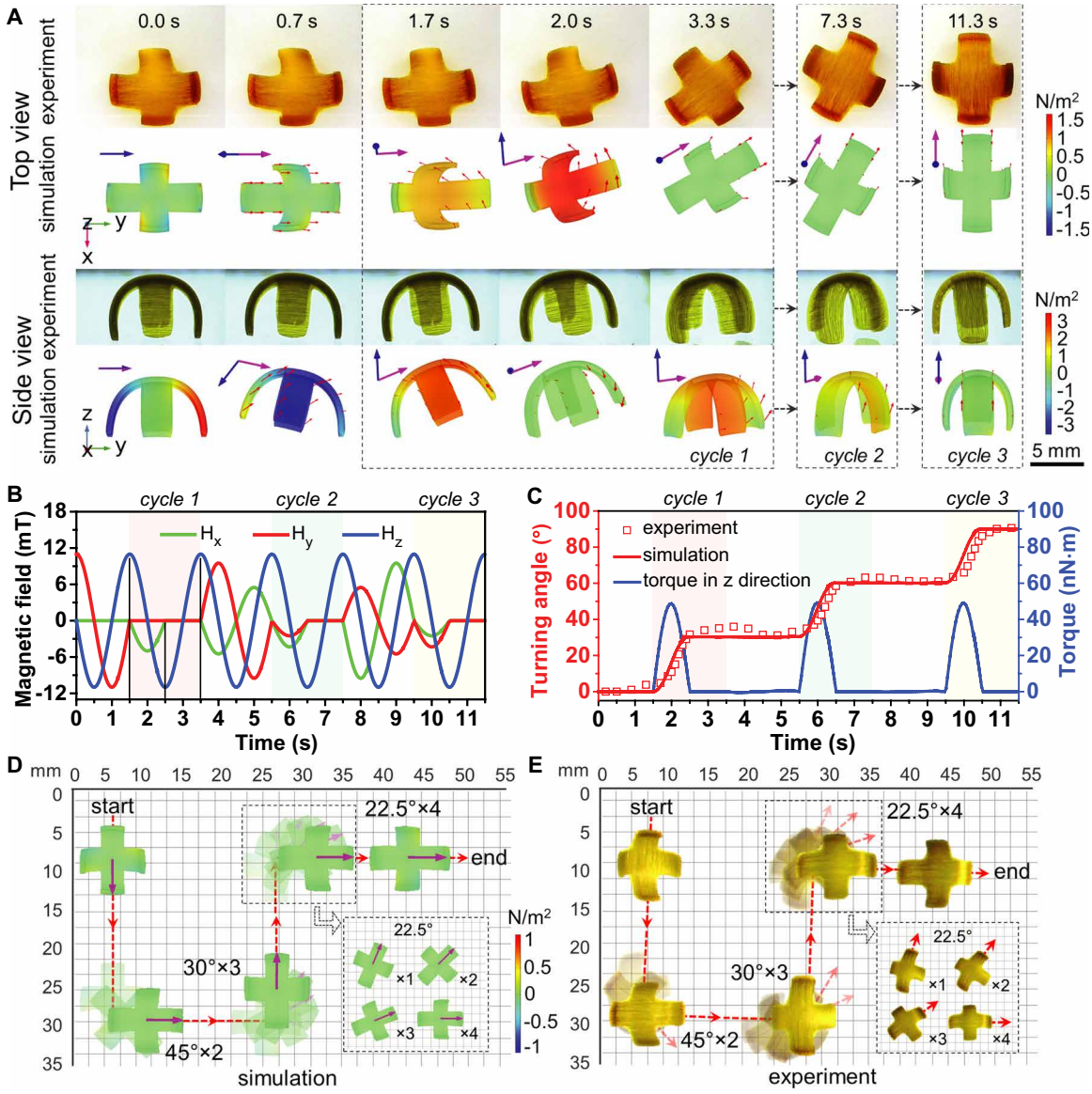

Fig. 3. Steering motion and path followed by samples under rotating magnetic fields. (**A**) Snapshots of three periods of steering motion from both experiment and simulation shown in the top view (top) and side view (bottom). Red arrows depict the instantaneous velocity field, blue arrows depict the direction of external rotating magnetic fields, purple arrows depict the direction of the average magnetization, and surface colors represent the *z* and *x* components of the magnetic torque density in the top and side views, respectively. (**B**) The *x*, *y*, and *z* components of the external rotating magnetic fields as functions of time. (**C**) Turning angle of the hydrogel robot from the experiment (red square) and the simulation (red line) and the *z* component of the total magnetic torque (blue line). Arbitrary path of the hydrogel from simulations (**D**) and experiment (**E**). The surface colors represent the *z* component of the magnetic torque density; dashed red line indicates the motion trajectory; magenta arrows indicate the direction of the average magnetization. Insets show a 90° turn in four 22.5° increments. "x1," "x2," "x3," and "x4" indicate the number of turning increments made while steering along a 90° turn.

to walk faster but rather accelerated flattening of bent samples (fig. S23). We also found that we can create objects with different walking modes by controlling the alignment direction of the nanowires during preparation of the Ni-hydrogel composites (fig. S24). Objects with nanowires aligned diagonally relative to their legs exhibited a walking motion by lifting two legs simultaneously under the rotating magnetic field (Fig. 5A and movie S8). Objects with nanowires aligned perpendicular to the films walk similarly to those with nanowires in the plane of the film but do not rotate their bodies when the magnetic field is reoriented from the *y*-*z* to *x*-*z* plane because of the lack of magnetic anisotropy (Fig. 5B and movie S8).

Cargo transport and release

In addition to walking across a flat plane, the hydrogel objects can also climb inclined surfaces (Fig. 6A and movie S9) and therefore displayed a different walking speed during the ascending and descending process (Fig. 6B). The hydrogel-metal hybrid samples can transport and release cargos using light and magnetic field exposure. Irradiating samples with high intensity light (4800 mW/cm^2) from below caused the hydrogel to curl into a spheroidal object, wrapping around an alginate hydrogel bead (cargo) that had been placed underneath it (Fig. 6C, top). We point out that substantial photothermal or photobleaching effects were not observed when

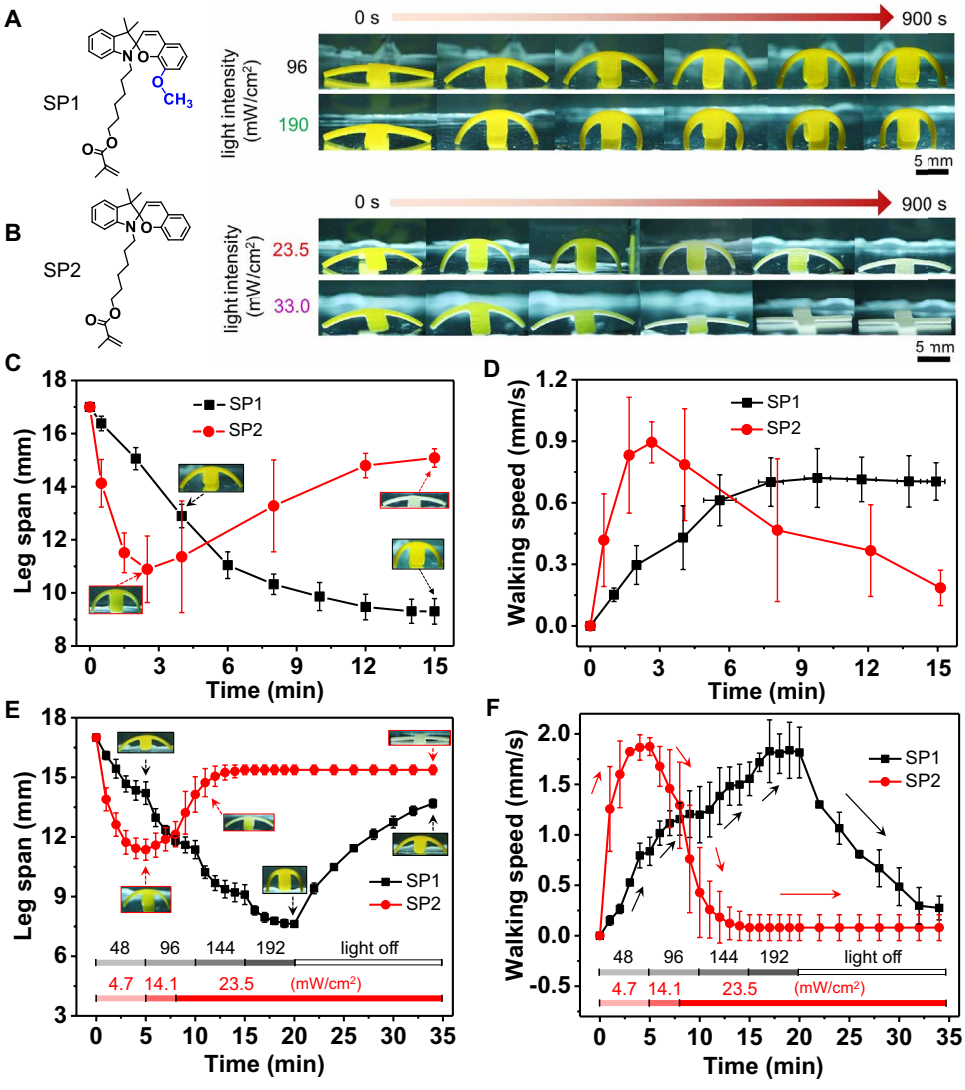

Fig. 4. Chemical design and bimodal control of the hydrogel robots. (**A** and **B**) Molecular structures of SP1 and SP2 and snapshots of the corresponding hydrogel robots under constant light irradiation over 900 s. (**C**) Leg span and (**D**) walking speed under irradiation with 96 mW/cm^2 for SP1 and 23.5 mW/cm^2 for SP2 (error bars represent SDs of data collected from three separate samples). (**E** and **F**) Variable light intensity applied over 2100 s to program leg span and walking speed, respectively. Black bar, four different light intensities (48, 96, 144, 192 mW/cm^2) were sequentially applied on SP1 samples every 5 min followed by a dark time for 15 min; red bar, three different light intensities (4.7, 14.1, and 23.5 mW/cm^2) were sequentially applied on SP2 samples for 5, 3, and 27 min, respectively.

using this short exposure to high intensity irradiation (fig. S25). The rolling motion of the ball-like object under a rotating magnetic field can be guided to different directions without dropping the alginate bead, allowing delivery of the cargo to any arbitrary destination (Fig. 6C, middle). By shining light continuously on the convex side of the object, we can eliminate the photoisomerization gradient to flatten the object first, followed by continuous irradiation from the bottom to create an opposing gradient, thus causing the object to bend up and release its cargo (Fig. 6C, bottom, and movie S10). In addition to using the rolling motion, our robot was also able to transport cargo using the walking motion. Because the MCH^+ is positively charged, the hydrogel robots can transport negatively charged cargo (an alginate bead) adhered to the top of the object through electrostatic attractions and deliver the cargo to any destination by walking and subsequent release by fast spinning (Fig. 6D and movie S10). These results offer proof of concept on the use of programmed light and magnetic fields to externally and remotely stimulate materials to transport and release cargo.

DISCUSSION

In this work, we have investigated the design of highly hydrated soft matter with the capability to respond to both light and magnetic fields to emulate locomotion and other functions observed in living organisms. This coupling is achieved by embedding rigid and macroscopically aligned ferromagnetic nanowires in a soft photoactive hydrogel. Compared with conventional polymers or liquid crystal elastomers (LCEs) that have been widely investigated, hydrogels offer great potential in biorelated applications because of their high water content and mechanical similarity to soft tissues. At the same time, the high aspect ratio of the Ni nanowires used to create the experimental materials allows the possibility of aligning the magnetic scaffold of the hydrogels. Thus, these hybrid materials have potential as systems that can be designed to have anisotropic properties. In this context, the common spherical and irregularly shaped magnetic particles (such as NdFeB) used in previous work lack well-defined shapes and magnetic anisotropy. In those earlier systems, a high content of the magnetic component [~10 weight % (wt %)] or a large magnetic field is required to activate a considerable response. In contrast, a very low content of aligned Ni nanowires (0.5 wt %) is sufficient in the hybrid hydrogels to generate a large magnetic response for robotic functions using a relatively weak magnetic field strength (≤16 mT). This advantage is supported by the product of the weight percentage of magnetic material and the applied field strength in our system, which is about three times lower than those used with previous systems (see the Supplementary Materials for details). Also, although the responses of our system to light and magnetic fields are driven by different mechanisms, they are interestingly coupled strongly via elastic deformation. The magnetic response depends on the geometry induced by photo-actuation (light direction, intensity, and irradiation time), whereas the magnetic response only appears to affect photo-actuation by changing the object's orientation with respect to incident light (fig. S26). As demonstrated above, chemical changes in the photoswitching molecules can also alter the programmable shape changes upon light exposure and in this way change the magnetically driven robotic functions. The photoswitching

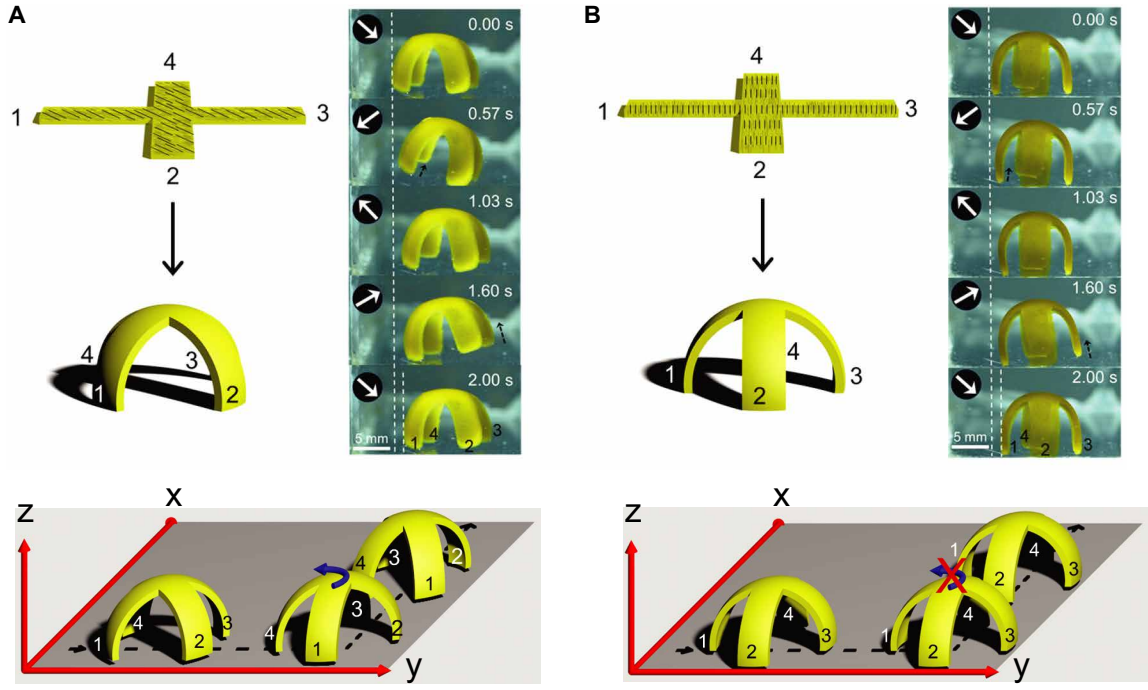

Fig. 5. Walking modes of the hydrogel robots in response to nanowire orientation. (**A**) Top, schematic representation of a cross-shaped hydrogel object irradiated from below with the Ni nanowires aligned diagonally, and photographs at different times (indicated at the upper right corner) of the hydrogel robot after irradiation walking from left to right for one cycle by lifting two legs simultaneously (1, 4) or (2, 3); bottom, schematic representation of the object rotating its body 90° counterclockwise when the rotation direction of the magnetic field changes from the *y*-*z* plane to the *x*-*z* plane. (**B**) Top, schematic representation of a cross-shaped hydrogel object irradiated from below with the Ni nanowires aligned perpendicular to the thickness direction, and photographs of the robots as in (A) but alternating the lift of legs 1 and 3 (white arrows indicate the direction of magnetic fields, and black dashed arrows indicate the lifting of the robot legs); bottom, schematic representation of the walking hydrogel robot showing that this orientation of the Ni nanowires does not lead to rotation of the robot's body when the magnetic field changes to the *x*-*z* plane.

approach via molecular isomerization offers the advantage of activation using relatively low light intensity (*25*, *27*, *34*). This is in contrast to the commonly used photothermal agents, which require high intensity light (*21*, *35*, *36*).

In miniaturized form, the materials developed in this work could be potentially used to transport and release cargoes in aqueous media through narrow passages with complex routes. In the experiments reported here, a rotating external field precessing at a 90° angle to the walking direction was selected because it maximizes the magnetic torque that drives actuation when the nanowires are aligned along the bending direction of the hydrogel. However, the actuation mechanisms investigated here could be used in the future to explore other modes of locomotion and functions by designing objects with other shapes and fields precessing at other angles with respect to the magnetization of the nanowires. The coupling principle between shape-morphing and responsive actuation developed here provides a general framework to create more complex bioinspired motions and functions.

Given the hydrogel nature of our materials, they can potentially collect molecular components from aqueous solutions and deliver them at another point by expelling water. Future directions could also include developing much smaller objects for drug delivery in tissues or to specific cells. In this respect, our understanding of the synergy between light and magnetic actuation will be important in design geometries suited for swimming and locomotion in low Reynolds number environments (*37*). The walking mechanism reported here can occur on any flat or inclined surface without relying on ratchets, which is comparable with previous photothermal (*38*), thermal (*39*), or electrically (*40*, *41*) driven walkers. The walking speed reached in our system (~2 mm/s) is fast from the perspective of previously observed light-induced locomotion but is comparable with other examples of magnetic actuation. However, we point out that in our system exposure of the objects to photons and the magnetic field are physically inseparable factors in the observed actuation. As we approach the walking speed in biologically relevant systems (~1 body length per second), the walking speed of our systems (~0.3 body length per second) is comparable or lower than that of light-actuated robots (*20*, *42*), which is limited by the viscous drag from the liquid environment and surface friction. With increasing walking speed, the viscous drag creates higher resistance forces, and slippage occurs during walking because of insufficient friction with the surface. Given the possibility to match the mechanical properties and water content of molecularly designed hydrogels to those of cells and tissues, these systems may allow us to recreate in synthetic robots the locomotion modes and other actuation behaviors observed in living organisms. We conclude that by theoretically integrating magnetoelasticity, polymer physics, and photochemical kinetics, we learned how to control locomotion and shape changes in soft materials responding to both light and magnetic fields.

MATERIALS AND METHODS

Materials

All chemicals used for SP synthesis were purchased from Sigma-Aldrich, Thermo Fisher Scientific, or other commercial companies and used directly without any purification unless mentioned. Anodic aluminum oxide membranes were purchased from Whatman Anodisc

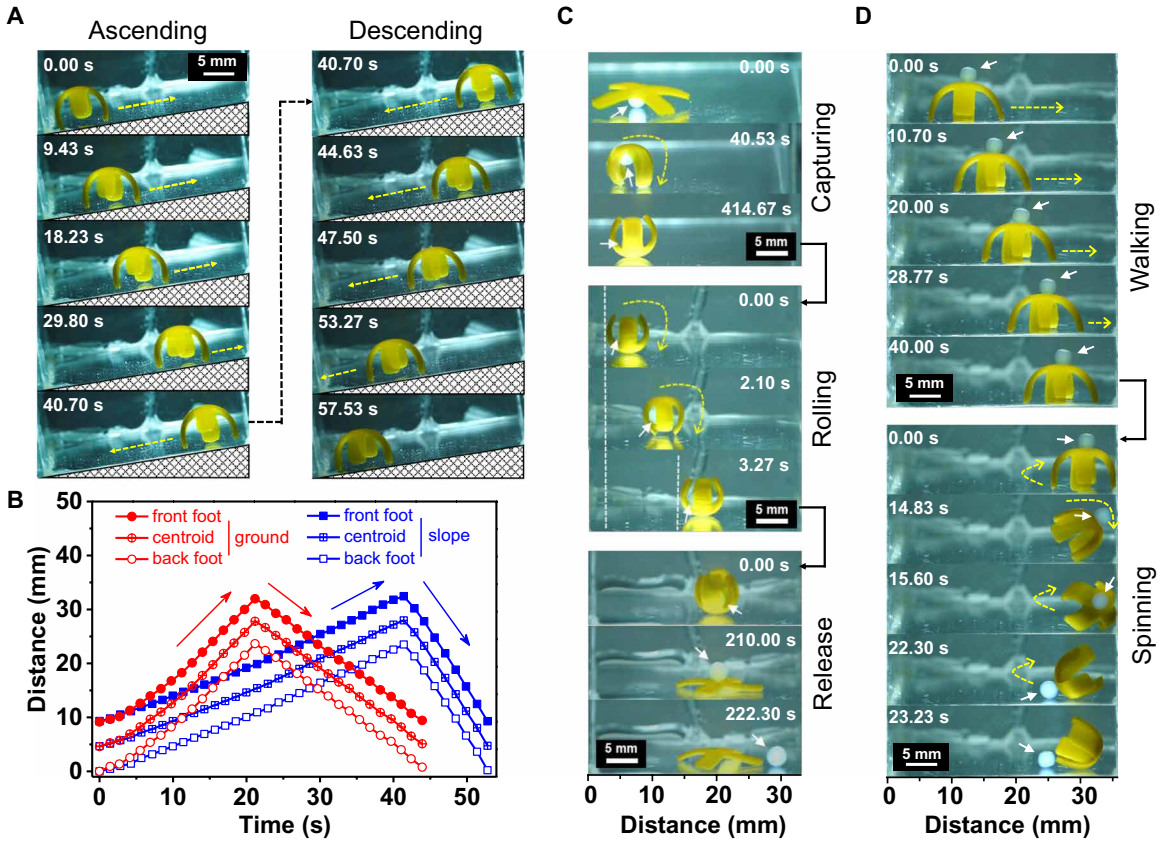

Fig. 6. Hydrogel robots performing tasks under rotating magnetic fields. (**A**) Photographs of ascending (left) and descending (right) hydrogel objects containing the SP1 moiety on a glass surface with an inclined angle of 9° and exposed to a magnetic field rotating in the *y*-*z* plane (the time at which each photograph was taken is indicated in the upper left-hand corner). (**B**) Plot of the position of the centroid, front and back feet of hydrogel objects as a function of time when robots walk on an inclined surface (blue) or a flat surface (red) but exposed to the same rotating magnetic field. (**C**) Starting at the top, sequential photographs (see times at upper right corner) show an alginate bead (white arrow) initially underneath a robot in the flattened state and subsequently captured when light from below bends the robot; the robot is then transported by a rolling motion under a magnetic field; and irradiation from the bottom exposes and releases the alginate cargo. (**D**) Time sequence photographs (see times at upper left corner) showing an alginate bead initially adhered to the top of a hydrogel object, then transported by walking motion, and subsequently released by fast spinning using the magnetic field.

(filter membranes, 0.02 μm pore size, 47 mm diameter, polypropylene support ring; GE Healthcare 68095502). Nickel electroplating solutions were purchased from Alfa Aesar (2026 Nickel plating solution, semi-bright finish). Nickel nanoparticles (200 nm diameter, 99.5% purity) were purchased from US Research Nanomaterials Inc. and used as received. The ultraviolet (UV)–curable resin was purchased from Loon Outdoors (UV Clear Fly Finish Thick), and the white-light light-emitting diodes (LEDs) were purchased from Chanzon (6000 to 6500 K color temperature; Amazon ASIN B01DBZHUXA). The NdFeB rare earth magnets used during hydrogel preparation were purchased from Applied Magnets (6 inches by 2 inches by 1 inch NdFeB Grade N42 block, model no. NB085-5), and the gaussmeter was purchased from AlphaLab (model VGM). The power and energy meter were purchased from Thorlabs (Digital Handheld Optical Power and Energy Meter Console, model PM100D), and a custom triaxial Helmholtz coil system was designed and fabricated by Micro Magnetics Inc. for all magnetic actuation and locomotion experiments (see the "Magnetic actuation" section for more details). Front- and side-view videos and photographs of photo-actuation and locomotion experiments were taken using a Nikon D5600 DSLR camera with a macro lens (Sigma 105-mm f/2.8 EX DG OS HSM Macro). Top-view videos and photographs were taken using an endoscopic camera (Dylviw 3 Meter Cable USB C Endoscope Inspection Camera, Amazon ASIN B075D52H7M) inserted into the magnetic chamber. Detailed synthesis and characterization of SP molecules are provided in the Supplementary Materials. Nickel nanowires were synthesized by adapting a protocol described by Bentley *et al.* (*43*), and detailed preparation protocols and characterization are given in the Supplementary Materials.

Hydrogel composite preparation

Thin films of hybrid hydrogels were prepared by photopolymerization of a solution containing monomers and Ni nanowires within glass molds. The thickness of hydrogel films (350 to 580 μm) was controlled using plastic spacers of known thickness adhered to the glass slides with a UV-curable resin (Loon Outdoors, UV Clear Fly Finish Thick). The polymerization solution was prepared in ethanol by adding *N*-isopropylacrylamide monomer [10 wt %, 4.40 mole percent (mol %)], *N*,*N*′-methylenebisacrylamide cross-linking monomer (0.68 wt %, 0.22 mol %), diphenyl(2,4,6-trimethylbenzoyl) phosphine oxide photoinitiator (0.5 wt %, 0.07 mol %), and the SP molecule (1.0 wt %, 0.14 mol %). The polymerization solution (200 μl) was centrifuged before use, then added to the dried Ni nanowires (1 mg), and sonicated to disperse them in a suspension containing 5 mg/ml

before pipetting into glass molds. The headspace of the mold was flushed for 10 min with argon saturated with ethanol vapor by flowing the gas through a bubbler filled with ethanol, thus mitigating any evaporation of the monomer solution. The molds were sealed with a UV-curable resin and briefly sonicated and shaken immediately before placing them in the photopolymerization setup.

The photopolymerization setup consisted of a transparent water bath kept at room temperature that held the molds upright between a pair of 100-W white-light LEDs (Chanzon, 6000 to 6500 K color temperature, Amazon ASIN B01DBZHUXA) mounted on aluminum fan–cooled heat sinks and 44-mm 60° lens (TX, Amazon ASIN B01D1LD68C). A pair of NdFeB rare earth magnets (Applied Magnets, 6 inches by 2 inches by 1 inches NdFeB Grade N42 block, model no. NB085-5) was mounted perpendicular to the LEDs to create a 25-mT magnetic field strength at the location of the water bath, as measured by a three-axis gaussmeter (AlphaLab Inc., model VGM). Samples with Ni nanowires oriented within the plane of the films were placed in the photopolymerization setup and oriented parallel to the direction of the magnetic field. The samples were prepolymerized by irradiation with the pair of 100-W LEDs to increase the solution's viscosity and reduce aggregation of the Ni nanowires. A period of 110 s was found to be the optimal prepolymerization time to reach a viscosity that is suitable for redispersion of the Ni nanowires using brief sonication and vigorous shaking. This way, we could allow the nanowires to align in the magnetic field without excessive aggregation during the rest of the polymerization process. After brief sonication and vigorous shaking, samples were immediately placed back into the setup and allowed to fully polymerize for an additional 8 min and 10 s. After polymerization, the gels were gently demolded using a razor blade and exposed to methanol for 10 min to wash out excess monomer and photoinitiator. Samples containing SP1 (or SP2) photoactive moieties were then immersed in 5 mM aqueous HCl for 40 or 90 min in the dark by covering them with aluminum foil to swell the hydrogels before actuation experiments. Samples were punched to the desired shape and Ni nanowire orientation in the swollen state using a high-strength acrylonitrile-butadiene-styrene punch that was 3D-printed using a Stratasys Connex 350 printer. The hydrogel film with chained Ni nanoparticles aligned parallel to the film was prepared following the same protocol described above. Samples with Ni nanowires aligned perpendicular to the films were prepared by orienting the molds perpendicular to the magnetic field between the NdFeB magnets. Unaligned samples were prepared following the same protocol but without use of the magnets.

Photo-actuation

Photo-actuation by irradiation with light from the top was carried out using gooseneck fiber optics combined with a white-light LED source. Photo-actuation from the bottom side of samples used a 100-W white LED (Bridgelux LED COB Vero 29 5000 K round, product no. BXRC-50C10K1-D-74) at variable currents placed under the sample chamber. Specifically, for walking motion experiments, SP1 samples were irradiated with a light intensity of 48 to 192 mW/cm^2 from below the hydrogel objects and an intensity of 4.7 to 33.0 mW/cm^2 for SP2 samples. For cargo capture experiments, SP1 samples were exposed to a light intensity of 4800 mW/cm^2 below the objects for 10 s. For cargo release, an intensity of 282 mW/cm^2 was used on the convex side of the bending object to flatten the object. After photo-actuation was complete, illumination for photography and videography was performed using a Bridgelux LED driven at 1 mA (~4.7 mW/cm^2) to minimize photoisomerization changes because of irradiation.

Magnetic actuation

Magnetic actuation experiments were performed using a custom-designed six-Helmholtz coil with a three-axis electromagnetic stage fabricated by Micro Magnetics Inc. with the following specifications: triaxial Helmholtz coils with effective diameters of 6, 11.3, and 17.5 inches for the x, y, and z axes, respectively; maximum DC magnetic field of ±30.0 mT for x axis, ±25.0 mT for y axis, and ±16.0 mT for z axis (working with controller); and physical dimensions of 19.5 inches (width) by 19.5 inches (depth) by 14 inches (height). For translational locomotion studies (rolling, flipping, and walking), a magnetic field rotating in either the x-z or y-z planes was used to cause translation in the x or y axes, respectively. Rotating magnetic fields were generated by driving perpendicular pairs of Helmholtz coils with a sinusoidal current amplitude and a phase lag of ±90° to control the direction of rotation. The x-z and y-z planes rotating magnetic fields had an amplitude of 16 mT.

Walking speed measurements

The cross-shaped hydrogel film containing aligned Ni nanowires was transferred to a water tank with dimensions of 40 mm (length) by 40 mm (width) by 75 mm (height) and exposed to a low-intensity DC magnetic field of 5.0 mT to align samples. Samples were then simultaneously exposed to a rotating magnetic field in the y-z plane and light irradiation from below the film, which triggered locomotion of the objects along the y axis of the chamber (the walking direction was reversed periodically to prevent the object from colliding with the walls of the water tank). Video recording throughout the entire process used a digital camera. The walking speed of the objects at one specific time point was recorded as an average of five walking steps. For each specific set of experimental conditions (frequency, strength of magnetic field, light intensity), the averages and SDs were obtained from measurements of three samples.

Cargo capture and release

A 10-s exposure to intense white LED illumination (4800 mW/cm^2) resulted in extremely rapid bending of a cross-shaped sample containing SP1 to create a strong gradient. Further irradiation with a much less intense LED (4.7 mW/cm^2) for 2 min resulted in curling of all four arms into a round, ball-like shape. An alginate particle (see the Supplementary Materials for a detailed description of the particle preparation) can be captured by the object when it curls into a spherical shape under light irradiation from below. This cargo was moved to a particular destination by rolling motion under the influence of rotating magnetic fields and released by irradiation on the convex side of the object to cause the object to gradually flatten and curl in the opposite direction.

Implementation details of simulations

The continuum model of the hydrogel robot was solved in two steps using the commercial finite-element software COMSOL. The first step calculates the deformation of the hydrogel robot under the influence of light, and the second step uses the deformed geometry as the reference configuration to calculate the dynamic behavior of the robot under an external magnetic field. For the first step, we used COMSOL's solid mechanics module and modeled the hydrogel as a

hyperelastic material to calculate its response to light. Because the photo component, U_{photo}, of the free energy density of the material depends on r_{sp} (the concentration of chromophores in SP form), the general form partial differential equation module of COMSOL was also used to calculate the light intensity and hence r_{sp} in the bulk of the material. For the second part of the simulation, the magnetic field was solved via the AC/DC module of COMSOL. The model developed for the fiber-reinforced magnetoelastic materials was implemented as a user-defined hyperelastic model in the Structural Mechanics module of COMSOL. The contribution from asymmetric magnetic Cauchy stress tensor $\boldsymbol{\sigma}_m$ was implemented via the weak contribution functionality of COMSOL. The contacts between the hydrogel robot and the floor are assumed to be nonslippery, and the contact events are detected via the Events module of COMSOL, which triggers time-dependent nonslippery boundary conditions. Besides, both volumetric gravitational and frictional forces were added into the continuum model to take into account the effect of gravity and the viscosity of the liquid environment, respectively.

SUPPLEMENTARY MATERIALS

robotics.sciencemag.org/cgi/content/full/5/49/eabb9822/DC1

Text

Fig. S1. Scanning electron microscopy (SEM) image of Ni nanowires, 200 nm in diameter and 8 to 10 μm in length.

Fig. S2. Characterization of the alignment of Ni nanowires during the two-step polymerization by optical microscopy.

Fig. S3. Optical microscope images of SP1 hydrogel-metal hybrid materials with rotating magnetic field (0.5 Hz, 15.0 mT, rotating in the *y-z* plane) off (left) and on (right).

Fig. S4. Characterization of the alignment of Ni nanowires embedded in the hydrogel using optical and scanning electron microscopy.

Fig. S5. Characterization of unaligned Ni nanowires embedded in the hydrogel matrix.

Fig. S6. Characterization of chained up Ni nanoparticles embedded in the hydrogel matrix.

Fig. S7. Superconducting quantum interference device (SQUID) measurements of different hydrogels.

Fig. S8. Volume change by light irradiation.

Fig. S9. Reversibility test of photo-actuation.

Fig. S10. Linear regime of the magnetic response of the Ni nanowires.

Fig. S11. Calibration of the elastic parameters from the DMA measurement after light irradiation.

Fig. S12. Benchmark of the fiber-reinforced magnetoelastic model using numerical and analytical solutions.

Fig. S13. Characterization of mechanical properties for hydrogel film samples after equilibrated in 5 mM HCl in the dark with Ni nanowires (0.5 wt %) aligned parallel or perpendicular to the plane of the films.

Fig. S14. Plot of G′ and G″ of samples before and after photo-actuation.

Fig. S15. Light-induced bending directions of the hydrogel squares (10 mm × 10 mm × 0.5 mm, L × W × T) containing aligned Ni nanowires (0.5 wt %) were affected by the mechanical anisotropy caused by the aligned Ni nanowires.

Fig. S16. Photographs of control hydrogels containing chained up Ni nanoparticles or unaligned Ni nanowires under the same magnetic fields.

Fig. S17. Optimization of the length of stabilizing arms.

Fig. S18. Absorbance spectra of SP1 and SP2 upon light irradiation.

Fig. S19. Absorbance spectra of SP1 and SP2 in the dark.

Fig. S20. Measured bending angle of hydrogels with varying light intensities.

Fig. S21. Measured leg span and walking speed of hydrogels containing SP1 and SP2 as a function of irradiation time.

Fig. S22. Hydrogel objects containing SP1 moiety bend up gradually controlled by programmed sequences of light intensity (48 to 192 mW/cm^2) irradiating from the bottom and flatten when light is off.

Fig. S23. Hydrogel objects containing SP2 moiety bend up in 5 min when irradiating with a bottom light (4.7 mW/cm^2) and gradually flatten when irradiating with stronger light (14.1, 23.5 mW/cm^2) because of the elimination of hydrophobicity gradient.

Fig. S24. Preparation of hydrogel objects with different alignment directions.

Fig. S25. Measurement of possible photothermal effect and photobleaching after irradiation with a strong light for 10 s.

Fig. S26. Effect of magnetic field on the photo-actuation.

Movie S1. Photo-actuation and walking motion of hydrogel-metal hybrids containing the SP1 moiety.

Movie S2. Effects of stabilizing arm length on walking gait of hydrogel-metal hybrids containing the SP1 moiety.

Movie S3. Effects of magnetic field strength and frequency on walking gait of the hydrogel-metal hybrids containing the SP1 moiety.

Movie S4. Walking gait of hydrogel-metal hybrids (SP1) with a reduced size.

Movie S5. Steering motion of the hydrogel-metal hybrids made of SP1 from experiment (left) and simulation (right).

Movie S6. Path following of hydrogel-metal hybrids from both simulation and experiment.

Movie S7. Chemical design and bimodal control of hydrogel-metal hybrids.

Movie S8. Walking gait of hydrogel-metal hybrids made of SP1 containing diagonally aligned and perpendicularly aligned Ni nanowires.

Movie S9. Climbing an inclined surface by hydrogel-metal hybrids made of SP1.

Movie S10. Cargo capture, transport, and release by hydrogel-metal hybrids made of SP1.

References (*44*–*50*)

REFERENCES AND NOTES

1. M. Wehner, R. L. Truby, D. J. Fitzgerald, B. Mosadegh, G. M. Whitesides, J. A. Lewis, R. J. Wood, An integrated design and fabrication strategy for entirely soft, autonomous robots. *Nature* **536**, 451–455 (2016).
2. S.-J. Park, M. Gazzola, K. S. Park, S. Park, V. di Santo, E. L. Blevins, J. U. Lind, P. H. Campbell, S. Dauth, A. K. Capulli, F. S. Pasqualini, S. Ahn, A. Cho, H. Yuan, B. M. Maoz, R. Vijaykumar, J. W. Choi, K. Deisseroth, G. V. Lauder, L. Mahadevan, K. K. Parker, Phototactic guidance of a tissue-engineered soft-robotic ray. *Science* **353**, 158–162 (2016).
3. A. S. Weingarten, R. V. Kazantsev, L. C. Palmer, M. McClendon, A. R. Koltonow, A. P. S. Samuel, D. J. Kiebala, M. R. Wasielewski, S. I. Stupp, Self-assembling hydrogel scaffolds for photocatalytic hydrogen production. *Nat. Chem.* **6**, 964–970 (2014).
4. H. Yang, B. S. Yeow, Z. Li, K. Li, T.-H. Chang, L. Jing, Y. Li, J. S. Ho, H. Ren, P.-Y. Chen, Multifunctional metallic backbones for origami robotics with strain sensing and wireless communication capabilities. *Sci. Robot.* **4**, eaax7020 (2019).
5. R. Dreyfus, J. Baudry, M. L. Roper, M. Fermigier, H. A. Stone, J. Bibette, Microscopic artificial swimmers. *Nature* **437**, 862–865 (2005).
6. J. M. Dempster, P. Vazquez-Montejo, M. Olvera de la Cruz, Contractile actuation and dynamical gel assembly of paramagnetic filaments in fast precessing fields. *Phys. Rev. E* **95**, 052606 (2017).
7. W. Hu, G. Z. Lum, M. Mastrangeli, M. Sitti, Small-scale soft-bodied robot with multimodal locomotion. *Nature* **554**, 81–85 (2018).
8. Y. Kim, H. Yuk, R. Zhao, S. A. Chester, X. Zhao, Printing ferromagnetic domains for untethered fast-transforming soft materials. *Nature* **558**, 274–279 (2018).
9. J. Cui, T.-Y. Huang, Z. Luo, P. Testa, H. Gu, X.-Z. Chen, B. J. Nelson, L. J. Heyderman, Nanomagnetic encoding of shape-morphing micromachines. *Nature* **575**, 164–168 (2019).
10. Y. Kim, G. A. Parada, S. Liu, X. Zhao, Ferromagnetic soft continuum robots. *Sci. Robot.* **4**, eaax7329 (2019).
11. T. Xu, J. Zhang, M. Salehizadeh, O. Onaizah, E. Diller, Millimeter-scale flexible robots with programmable three-dimensional magnetization and motions. *Sci. Robot.* **4**, eaav4494 (2019).
12. J. A.-C. Liu, J. H. Gillen, S. R. Mishra, B. A. Evans, J. B. Tracy, Photothermally and magnetically controlled reconfiguration of polymer composites for soft robotics. *Sci. Adv.* **5**, eaaw2897 (2019).
13. L. Ionov, Hydrogel-based actuators: Possibilities and limitations. *Mater. Today* **17**, 494–503 (2014).
14. Y. Zhao, C. Xuan, X. Qian, Y. Alsaid, M. Hua, L. Jin, X. He, Soft phototactic swimmer based on self-sustained hydrogel oscillator. *Sci. Robot.* **4**, eaax7112 (2019).
15. W. Francis, A. Dunne, C. Delaney, L. Florea, D. Diamond, Spiropyran based hydrogels actuators—Walking in the light. *Sens. Actuat. B Chem.* **250**, 608–616 (2017).
16. C. Li, A. Iscen, L. C. Palmer, G. C. Schatz, S. I. Stupp, Light-driven expansion of spiropyran hydrogels. *J. Am. Chem. Soc.* **142**, 8447–8453 (2020).
17. Y. S. Kim, M. Liu, Y. Ishida, Y. Ebina, M. Osada, T. Sasaki, T. Hikima, M. Takata, T. Aida, Thermoresponsive actuation enabled by permittivity switching in an electrostatically anisotropic hydrogel. *Nat. Mater.* **14**, 1002–1007 (2015).
18. S. Maeda, Y. Hara, T. Sakai, R. Yoshida, S. Hashimoto, Self-walking gel. *Adv. Mater.* **19**, 3480–3484 (2007).
19. D. Han, C. Farino, C. Yang, T. Scott, D. Browe, W. Choi, J. W. Freeman, H. Lee, Soft robotic manipulation and locomotion with a 3D printed electroactive hydrogel. *ACS Appl. Mater. Inter.* **10**, 17512–17518 (2018).
20. A. Mourran, H. Zhang, R. Vinokur, M. Moller, Soft microrobots employing nonequilibrium actuation via plasmonic heating. *Adv. Mater.* **29**, 1604825 (2017).
21. I. K. Han, T. Chung, J. Han, Y. S. Kim, Nanocomposite hydrogel actuators hybridized with various dimensional nanomaterials for stimuli responsiveness enhancement. *Nano Converg.* **6**, 18 (2019).

22. T. Caykara, D. Yörük, S. Demirci, Preparation and characterization of poly(*N*-tert-butylacrylamide-*co*-acrylamide) ferrogel. *J. Appl. Polym. Sci.* **112**, 800–804 (2009).
23. J. Tang, Z. Tong, Y. Xia, M. Liu, Z. Lv, Y. Gao, T. Lu, S. Xie, Y. Pei, D. Fang, T. J. Wang, Super tough magnetic hydrogels for remotely triggered shape morphing. *J. Mater. Chem. B* **6**, 2713–2722 (2018).
24. Q. Li, A. P. H. J. Schenning, T. J. Bunning, Light-responsive smart soft matter technologies. *Adv. Opt. Mater.* **7**, 1901160 (2019).
25. M. M. Russew, S. Hecht, Photoswitches: From molecules to materials. *Adv. Mater.* **22**, 3348–3360 (2010).
26. A. H. Gelebart, D. Jan Mulder, M. Varga, A. Konya, G. Vantomme, E. W. Meijer, R. L. B. Selinger, D. J. Broer, Making waves in a photoactive polymer film. *Nature* **546**, 632–636 (2017).
27. R. Klajn, Spiropyran-based dynamic materials. *Chem. Soc. Rev.* **43**, 148–184 (2014).
28. C. Li, A. Iscen, H. Sai, K. Sato, N. A. Sather, S. M. Chin, Z. Álvarez, L. C. Palmer, G. C. Schatz, S. I. Stupp, Supramolecular–covalent hybrid polymers for light-activated mechanical actuation. *Nat. Mater.* **19**, 900–909 (2020).
29. J. W. Chen, F. K.-C. Leung, M. C. A. Stuart, T. Kajitani, T. Fukushima, E. van der Giessen, B. L. Feringa, Artificial muscle-like function from hierarchical supramolecular assembly of photoresponsive molecular motors. *Nat. Chem.* **10**, 132–138 (2018).
30. F. K.-C. Leung, T. Kajitani, M. C. A. Stuart, T. Fukushima, B. L. Feringa, Dual-controlled macroscopic motions in a supramolecular hierarchical assembly of motor amphiphiles. *Angew. Chem. Int. Ed.* **58**, 10985–10989 (2019).
31. B. Gao, L. Qiao, J. Wang, Q. Liu, F. Li, J. Feng, D. Xue, Microwave absorption properties of the Ni nanowires composite. *J. Phys. D Appl. Phys.* **41**, 235005 (2008).
32. O. Kuksenok, A. C. Balazs, Modeling the photoinduced reconfiguration and directed motion of polymer gels. *Adv. Funct. Mater.* **23**, 4601–4610 (2013).
33. G. Y. Qiu, T. J. Pence, Remarks on the behavior of simple directionally reinforced incompressible nonlinearly elastic solids. *J. Elast.* **49**, 1–30 (1997).
34. F. Lancia, A. Ryabchun, N. Katsonis, Life-like motion driven by artificial molecular machines. *Nat. Rev. Chem.* **3**, 536–551 (2019).
35. E. Wang, M. S. Desai, S. W. Lee, Light-controlled graphene-elastin composite hydrogel actuators. *Nano Lett.* **13**, 2826–2830 (2013).
36. H. Shahsavan, A. Aghakhani, H. Zeng, Y. Guo, Z. S. Davidson, A. Priimagi, M. Sitti, Bioinspired underwater locomotion of light-driven liquid crystal gels. *Proc. Natl. Acad. Sci. U.S.A.* **117**, 5125–5133 (2020).
37. B. Behkam, M. Sitti, Design methodology for biomimetic propulsion of miniature swimming robots. *J. Dyn. Sys. Meas. Control.* **128**, 36–43 (2005).
38. I. Rehor, C. Maslen, P. G. Moerman, B. G. P. van Ravensteijn, R. van Alst, J. Groenewold, H. B. Eral, W. K. Kegel, Photoresponsive hydrogel microcrawlers exploit friction hysteresis to crawl by reciprocal actuation. *Soft Robot* , (2020).
39. O. J. Sul, M. R. Falvo, R. M. Taylor, S. Washburn, R. Superfine, Thermally actuated untethered impact-driven locomotive microdevices. *Appl. Phys. Lett.* **89**, 203512 (2006).
40. D. Morales, E. Palleau, M. D. Dickey, O. D. Velev, Electro-actuated hydrogel walkers with dual responsive legs. *Soft Matter* **10**, 1337–1348 (2014).
41. B. R. Donald, C. G. Levey, C. D. McGray, I. Paprotny, D. Rus, An untethered, electrostatic, globally controllable MEMS micro-robot. *J. Microelectromech. Syst.* **15**, 1–15 (2006).
42. H. Zeng, P. Wasylczyk, C. Parmeggiani, D. Martella, M. Burresi, D. S. Wiersma, Light-fueled microscopic walkers. *Adv. Mater.* **27**, 3883–3887 (2015).
43. A. K. Bentley, M. Farhoud, A. B. Ellis, A.-M. L. Nickel, G. C. Lisensky, W. C. Crone, Template synthesis and magnetic manipulation of nickel nanowires. *J. Chem. Educ.* **82**, 765–768 (2005).
44. T. Satoh, K. Sumaru, T. Takagi, K. Takai, T. Kanamori, Isomerization of spirobenzopyrans bearing electron-donating and electron-withdrawing groups in acidic aqueous solutions. *Phys. Chem. Chem. Phys.* **13**, 7322–7329 (2011).
45. M. Dehghany, H. H. Zhang, R. Naghdabadi, Y. H. Hu, A thermodynamically-consistent large deformation theory coupling photochemical reaction and electrochemistry for light-responsive gels. *J. Mech. Phys. Solids* **116**, 239–266 (2018).
46. M. Doi, Gel dynamics. *J. Phys. Soc. Jpn.* **78**, 052001 (2009).
47. L. Dorfmann, R. W. Ogden, *Nonlinear Theory of Electroelastic and Magnetoelastic Interactions* (Springer, 2014).
48. M. M. Attard, Finite strain-isotropic hyperelasticity. *Int. J. Solids Struct.* **40**, 4353–4378 (2003).
49. R. Bustamante, Transversely isotropic nonlinear magneto-active elastomers. *Acta Mech.* **210**, 183–214 (2010).
50. J. Bonet, R. D. Wood, *Nonlinear Continuum Mechanics for Finite Element Analysis* (Cambridge Univ. Press, 2008).

Acknowledgments: We thank J. E. Kupferberg for preparation of the alginate beads and M. Seniw for schematic illustrations. This work made use of the IMSERC at Northwestern University, which has received support from the NIH (1S10OD012016-01/1S10RR019071-01A1), Soft and Hybrid Nanotechnology Experimental (SHyNE) Resource (NSF ECCS-1542205), the State of Illinois, and the International Institute for Nanotechnology (IIN). This work also made use of the MatCI Facility, which receives support from the MRSEC Program (NSF DMR-1720139) of the Materials Research Center at Northwestern University. The x-ray scattering experiment was performed at the DuPont-Northwestern-Dow Collaborative Access Team (DND-CAT) located at Sector 5 of the Advanced Photon Source (APS). DND-CAT is supported by Northwestern University, Dow Chemical Company, and DuPont de Nemours Inc., and APS is a U.S. Department of Energy (DOE) Office of Science User Facility operated for the DOE Office of Science by Argonne National Laboratory under contract no. DE-AC02-06CH11357. Data were collected using an instrument funded by the NSF under award no. 0960140. **Funding:** This work was supported by the Center for Bio-Inspired Energy Science (CBES), an Energy Frontier Research Center funded by the U.S. Department of Energy (DOE), Office of Science, Basic Energy Sciences under award number DE-SC0000989. **Author contributions:** C.L. and G.C.L. designed, synthesized, and characterized the hydrogel-metal hybrid materials; carried out most of the experiments; and wrote the manuscript. H.Y. developed the magnetoelastic theory and designed the program for controlling the robotic locomotion and wrote the manuscript. A.A. and S.L. developed and solved the light-responsive hydrogel theory and wrote the manuscript. V.L.D. and P.K.A. carried out the vibrating sample magnetometry (VSM) measurements and analyzed the data. H.S. performed the 2D x-ray scattering experiments. L.C.P. discussed and wrote the manuscript. N.A.S. constructed molds used for robotic function testing. T.J.P. and D.E.F. carried out the superconducting quantum interference device (SQUID) measurements. M.O.d.l.C. and S.I.S. directed the research and wrote the manuscript. All authors contributed to data analysis and manuscript preparation. **Competing interests:** The authors declare that they have no competing interests. **Data and materials availability:** All data needed to evaluate the conclusions in this manuscript are presented in the main text or the Supplementary Materials.

Submitted 31 March 2020
Accepted 12 November 2020
Published 9 December 2020
10.1126/scirobotics.abb9822

Citation: C. Li, G. C. Lau, H. Yuan, A. Aggarwal, V. L. Dominguez, S. Liu, H. Sai, L. C. Palmer, N. A. Sather, T. J. Pearson, D. E. Freedman, P. K. Amiri, M. Olvera de la Cruz, S. I. Stupp, Fast and programmable locomotion of hydrogel-metal hybrids under light and magnetic fields. *Sci. Robot.* **5**, eabb9822 (2020).

Fast and programmable locomotion of hydrogel-metal hybrids under light and magnetic fields

Chuang Li, Garrett C. Lau, Hang Yuan, Aaveg Aggarwal, Victor Lopez Dominguez, Shuangping Liu, Hiroaki Sai, Liam C. Palmer, Nicholas A. Sather, Tyler J. Pearson, Danna E. Freedman, Pedram Khalili Amiri, Monica Olvera de la Cruz and Samuel I. Stupp

Sci. Robotics **5**, eabb9822.
DOI: 10.1126/scirobotics.abb9822